ELSEVIER

Chemical Engineering Journal 85 (2002) 87–97

Chemical Engineering Journal

www.elsevier.com/locate/cej

Modeling of pulsed corona discharge process for the removal of nitric oxide and sulfur dioxide

Young Sun Mok [a,*], In-Sik Nam [b]

[a] *Department of Chemical Engineering, Cheju National University, Ara-dong 1, Cheju 690-756, South Korea*
[b] *Department of Chemical Engineering, Pohang University of Science and Technology, Pohang, Kyungbuk 790-784, South Korea*

Accepted 7 September 2001

Abstract

A positive pulsed corona discharge process was applied to the removal of sulfur dioxide and nitric oxide from a simulated flue gas stream, and a mathematical model was proposed to describe this process theoretically. The proposed model takes into account generation of radicals by pulsed corona discharge, followed by radical utilization for the removal of the pollutants. Radicals such as O, OH, N, H, etc. may be concerned in the removal of the pollutants. Their concentrations were derived by considering direct electron impact on the dissociation of gaseous molecules (O_2, N_2, H_2O) and subsequent excitation transfer reactions of excited oxygen atoms to produce O and OH radicals. The effects of various operating parameters such as feed gas flow rate, initial concentration, oxygen content, humidity, peak voltage and pulse repetition rate on the removal were examined. So as to establish the validity of the model, the calculated results were compared with the experimental data. Although some discrepancy between the calculated and experimental results was observed at high pulse repetition rate, the proposed model was found to properly predict the experimental data on the whole.

Keywords: Pulsed; Corona discharge; Mathematical model; Sulfur dioxide; Nitric oxide

1. Introduction

SO_2 and NO emitted from various sources, including power plants, iron and steel plants, paper mills and the like are the major cause of acid rain. There is a growing interest for flue gas cleaning by non-thermal plasma technologies characterized by low gas temperature and high electron temperature, one of which is a pulsed corona discharge process (PCDP). Compared to the other non-thermal plasma technologies using dc or ac corona discharge, PCDP is energy efficient because a large amount of energy goes into the production of energetic electrons rather than into gas heating, and the performance is good due to the large ionization region [1]. Since this process has many advantages over conventional technologies for flue gas cleaning, a lot of interest has recently been taken in this process [2–6].

The electrode structure of the corona reactor for the removal of SO_2 and NO can be either wire-to-cylinder or wire-to-plate [2,7]. For example, wire-to-cylinder type corona reactor consists of a cylinder and thin coaxial wire. The wire is usually connected to a positive high voltage with pulse width less than 1 μs, and the outer cylinder is grounded [7,8]. Therefore, the inner wire and outer cylinder act as anode and cathode, respectively. When the electric field generated from the positive pulse voltage is high enough to induce breakdown of gas, corona discharge starts from the inner wire (discharging electrode) by forming a number of corona streamers, and propagates toward the outer cylinder [2].

In the literature, there are several modeling studies on plasma discharge process applied to air pollution control [9–12]. Tamon et al. [9] have proposed the removal of electronegative impurities by electron attachment, and performed experiments for the removal of sulfur compounds and iodine to verify their concept. They correlated the experimental results to their model. Lowke and Morrow [10] have theoretically analyzed the role of various species in the removal of NO, NO_2 and SO_2 from flue gas for cases where pulsed positive voltages have been applied to electrostatic precipitators. They calculated the rate coefficients for electron dissociation of principal gaseous components, the rates of ionization and attachments, and the rates of excitation of the principal excited states, to find the removal mechanism of SO_2 and nitrogen oxides.

* Corresponding author. Tel.: +82-64-754-3682; fax: +82-64-755-3670.
E-mail address: smokie@cheju.cheju.ac.kr (Y.S. Mok).

1385-8947/02/$ – see front matter
PII: S1385-8947(01)00221-2

Nomenclature

$[C_j]_i$	concentration of jth component after ith pulsing (molecules/cm^3)
C_p	capacitance of the charging capacitor (pF)
e	electron
E	electric field (V/cm)
E_p	energy delivered to the reactor per pulse (J/pulse)
f	pulse repetition rate (Hz)
i	number of pulses accepted by gas stream
k_1–k_{31}	reaction rate constants in Tables 3 and 4 (cm^3/(molecules s))
k_{d1}–k_{d4}	dissociation reaction rate constants in reactions (1)–(4) (cm^3/(molecules s))
k_{e1}–k_{e4}	O(^{1}D) depletion rate constants in reactions (10)–(13) (cm^3/(molecules s))
M	three-body reaction partner (molecules/cm^3)
N_T	total number density (molecules/cm^3)
$[O]_d$	concentration of ground-state oxygen atom produced by electron–molecule collision (molecules/cm^3)
$[O(^1D)]_d$	concentration of excited oxygen atom produced by electron–molecule collision (molecules/cm^3)
$[OH]_d$	concentration of hydroxyl radical produced by electron–molecule collision (molecules/cm^3)
q_e	electron charge (C)
$R_{j,i}$	reaction rate of jth component at ith pulsing (molecules/(cm^3 s))
t	time (s)
T	temperature (K)
v_d	electron drift velocity (cm/s)
V_R	total reactor volume (cm^3)
$[\cdot]$	concentration (molecules/cm^3)

Greek letters

η_c	overall radical production efficiency by corona discharge (molecules/J)
η_d	radical production efficiency by direct electron dissociation impact (molecules/J)
τ	space time, ratio of reactor volume to gas flow rate (s)
τ_p	pulse period (s)

Subscripts

0	reactor inlet
i	ith pulsing
j	any component

A comparative assessment of three types of electrical discharge reactors such as pulsed corona, dielectric-barrier discharge and dielectric-pellet bed reactor was carried out by Penetrante et al. [11]. They conducted experiments for NO removal from NO and N_2 mixtures using the above three electrical discharge reactors, and compared experimental data with calculated results. Sun et al. [12] reported on a computational study of SO_2 and NO removal by dielectric-barrier discharge and discussed the parametric dependencies of SO_2 and NO removal efficiencies on the input conditions.

This study is aiming at developing a theoretical model capable of describing the behavior of the removal of NO_x and SO_2 in a pulsed corona discharge reactor. Concentrations of key radicals in this process were theoretically derived, and the governing equations of the model were solved using the concentrations of the radicals derived. The experiments were performed with a wire-cylinder type reactor and a homemade high voltage pulse generator. The experimental data obtained at a variety of conditions were compared with the calculation results to verify the validity of the proposed model.

2. Theory

2.1. Description of pulsed corona discharge process

The pulsed corona discharge is induced by the application of fast-rising narrow positive high voltage pulse to non-uniform electrode geometry. It develops by forming a number of streamers, the starting points of which are discrete and distributed over the surface of discharging wire [2,13,14]. The experimentally observed propagation velocity of streamer (from streak camera and photo-multiplier technique) in air is about 10^6 m/s [15]. Free electrons produced by pulsed corona discharge can be accelerated by an imposed electric field to gain energy. High energy electrons created by pulsed corona discharge are in the range of 5–10 eV (1 eV $= 1.6 \times 10^{-19}$ J) on the average [16]. During their drift, they can collide with various molecules and lose energy. The collisions of energetic electrons with oxygen, water vapor and nitrogen result in the formation of various active species [10,12,17]. These species with strong reactivity can react with a variety of gaseous pollutants such as SO_2 and NO, leading to the removal of them [8].

2.2. Radical production

Fig. 1 depicts the schematic of the removal mechanism of NO and SO_2 in a corona reactor. We divided the overall procedure into three steps to analyze this process theoretically. The production of important radicals associated with the removal may be initiated by collisions between energetic electrons and background molecules [10,12,17,18]. The electron impact processes on the dissociation of the background molecules considered are shown in Table 1. The dissociation rate coefficients k_{d1}–k_{d4} can be obtained from the solution of Boltzmann equation for the electron energy distribution and the appropriate cross-sections [19].

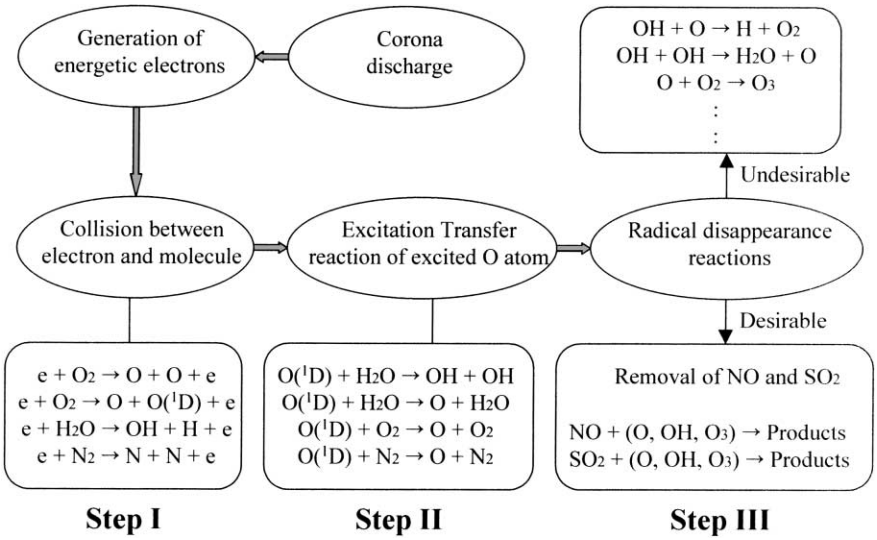

Fig. 1. Schematic of the removal mechanism of NO and SO_2.

We may define a production efficiency for a primary radical produced by direct electron–molecule collision as the number of atoms or radicals created per unit electrical discharge energy:

$$\eta_{d,OH} = \eta_{d,H} = \frac{k_{d1}[H_2O]}{q_e v_d N_T (E/N_T)} \quad (5)$$

$$\eta_{d,O} = \frac{(2k_{d2} + k_{d3})[O_2]}{q_e v_d N_T (E/N_T)} \quad (6)$$

$$\eta_{d,O(^1D)} = \frac{k_{d3}[O_2]}{q_e v_d N_T (E/N_T)} \quad (7)$$

$$\eta_{d,N} = \frac{2k_{d4}[N_2]}{q_e v_d N_T (E/N_T)} \quad (8)$$

where q_e is the electron charge (C), E the electric field (V/cm), v_d the electron drift velocity (cm/s), and N_T is the total number density (molecules/cm^3). The ratio of the electric field to the total number density (E/N_T) is known as the reduced electric field. It has widely been used in high voltage gas discharge because the characteristics of the corona discharge can be affected by the total number density as well as the electric field itself. In Eqs. (5)–(8), the concentrations of O_2, H_2O and N_2 that are the major components in the gas stream can be assumed to be always constant although small amounts of O_2, H_2O and N_2 are consumed by the dissociation.

The electron drift velocity v_d in Eqs. (5)–(8) can be expressed as a function of reduced electric field E/N_T [15]:

$$v_d = 3.2 \times 10^5 (E/N_T)^{0.8} \quad (9)$$

The excited atomic oxygen O(^{1}D) generated from reaction (3) in Table 1 can be depleted due to rapid quenching with background molecules such as N_2, O_2 and H_2O to give O and OH radicals [19,20]. The excitation transfer reactions are reported in Table 2. While most of OH radicals are contributed through charge-exchange reactions in the case of electron beam irradiation process, the OH formation in electrical discharge process is dominated by hydrogen abstraction from H_2O by O(^{1}D) under most conditions [20]. The electron beam has large electron energies (300–750 keV) enough to ionize neutral molecules, on the other hand, corona discharge generates electrons in the range of 5–10 eV [16]. Therefore, OH is dominantly produced through the neutral channel in corona discharge whereas this occurs through the ion channel in the electron beam irradiation process. If we assume that the electron–molecule collision and the depletion of the excited oxygen atom occur sequentially as depicted in Fig. 1, the depletion rate of O(^{1}D) can be written

Table 1
Production of radicals by electron–molecule collision processes

Collision process	Reaction number
$e + H_2O \xrightarrow{k_{d1}} OH + H + e$	(1)
$e + O_2 \xrightarrow{k_{d2}} O + O + e$	(2)
$e + O_2 \xrightarrow{k_{d3}} O + O(^1D) + e$	(3)
$e + N_2 \xrightarrow{k_{d4}} N + N + e$	(4)

Table 2
Production of radicals by excitation transfer reactions[a]

Reactions	Rate constants	Reaction number
$O(^1D) + H_2O \rightarrow OH + OH$	$k_{e1} = 2.2 \times 10^{-10}$	(10)
$O(^1D) + N_2 \rightarrow O + N_2$	$k_{e2} = 2.6 \times 10^{-11}$	(11)
$O(^1D) + O_2 \rightarrow O + O_2$	$k_{e3} = 3.8 \times 10^{-11}$	(12)
$O(^1D) + H_2O \rightarrow O + H_2O$	$k_{e4} = 1.2 \times 11^{-10}$	(13)

[a] k_{e1}–k_{e4} are at 300 K and their unit is in cm^3/(molecules s).

as follows:

$$-\frac{d[O(^1D)]}{dt} = \{(k_{e1}+k_{e4})[H_2O]+k_{e2}[N_2]+k_{e3}[O_2]\}[O(^1D)] \quad (14)$$

Since the concentrations of the major gas components such as O_2, N_2 and H_2O can be assumed to be constant, Eq. (14) can easily be integrated to give

$$[O(^1D)] = [O(^1D)]_d \exp[-\{(k_{e1}+k_{e4})[H_2O]+k_{e2}[N_2]+k_{e3}[O_2]\}t] \quad (15)$$

where $[O(^1D)]_d$ is the concentration of $O(^1D)$ produced by electron–molecule collision process.

The production rate of OH radical by hydrogen abstraction from H_2O by excited oxygen atom $O(^1D)$ is equated as follows:

$$\frac{d[OH]}{dt} = 2k_{e1}[O(^1D)][H_2O] \quad (16)$$

Similarly, from the reactions (10)–(13), the production rate of ground-state oxygen atom by $O(^1D)$ depletion reactions can be written as

$$\frac{d[O]}{dt} = \{k_{e2}[N_2]+k_{e3}[O_2]+k_{e4}[H_2O]\}[O(^1D)] \quad (17)$$

We can rewrite Eqs. (16) and (17) by substituting Eq. (15) for $O(^1D)$ concentration and integrating with respect to time:

$$[OH] = 2k_{e1}[H_2O][O(^1D)]_d \times \frac{\exp[-\{(k_{e1}+k_{e4})[H_2O]+k_{e2}[N_2]+k_{e3}[O_2]\}t]-1}{-\{(k_{e1}+k_{e4})[H_2O]+k_{e2}[N_2]+k_{e3}[O_2]\}} + [OH]_d \quad (18)$$

$$[O] = \{k_{e2}[N_2]+k_{e3}[O_2]+k_{e4}[H_2O]\}[O(^1D)]_d \times \frac{\exp[-\{(k_{e1}+k_{e4})[H_2O]+k_{e2}[N_2]+k_{e3}[O_2]\}t]-1}{-\{(k_{e1}+k_{e4})[H_2O]+k_{e2}[N_2]+k_{e3}[O_2]\}} + [O]_d \quad (19)$$

where $[OH]_d$ and $[O]_d$ are the concentrations of OH and O produced by electron–molecule collision processes, respectively.

The exponential term in Eqs. (18) and (19) approaches zero within about 5 ns, i.e. we can assume that the productions of OH and O via the excitation transfer reactions of $O(^1D)$ occur instantaneously. In such a case, the exponential term can be eliminated from Eqs. (18) and (19). Rewriting these equations in terms of the number of species created per unit discharge energy, the overall radical production efficiencies are given by

$$\eta_{c,OH} = \frac{2k_{e1}[H_2O]\eta_{d,O(^1D)}}{(k_{e1}+k_{e4})[H_2O]+k_{e2}[N_2]+k_{e3}[O_2]} + \eta_{d,OH} \quad (20)$$

$$\eta_{c,O} = \frac{(k_{e2}[N_2]+k_{e3}[O_2]+k_{e4}[H_2O])\eta_{d,O(^1D)}}{(k_{e1}+k_{e4})[H_2O]+k_{e2}[N_2]+k_{e3}[O_2]} + \eta_{d,O} \quad (21)$$

By the scheme in Fig. 1, H and N radicals are produced only via direct electron dissociation impact as in Table 1. The average concentrations of O, OH, H and N radicals produced per single pulse can be written using the radical production efficiencies above:

$$[OH]_c = \eta_{c,OH}\frac{E_p}{V_R}; \quad [O]_c = \eta_{c,O}\frac{E_p}{V_R};$$
$$[H]_c = \eta_{d,H}\frac{E_p}{V_R}; \quad [N]_c = \eta_{d,N}\frac{E_p}{V_R} \quad (22)$$

where E_p is the discharge energy delivered per pulse and V_R the volume of the plasma reactor.

The propagation speed of the corona streamer toward the cathode is as high as one percent of light speed [15,21], nevertheless, the concentrations of radicals generated cannot perfectly be homogeneous over the reactor volume due to the nature of spatial non-uniformity of the corona streamers. Therefore, Eq. (22) corresponds to the concentration averaged over the reactor volume.

2.3. Removal mechanism

Table 3 summarizes the reactions considered and the related rate coefficients where the symbol, *M*, in the reaction rate constants refers to any major gas component in three-body reactions. The rate constants in Table 3 are cited from Baulch et al. [22] and Atkinson et al. [23].

Competition between oxidation and reduction can explain the conversion of NO although the predominant removal path is dependent on the composition of feed gas stream. NO can be oxidized to NO_2 by O, OH, HO_2 and O_3 as described in Table 3. NO_2 produced can be further oxidized to nitric acid by OH radical according to the reaction (26). The reduction of NO to N_2 is mainly effected by N radical as the reaction (33). N radical is also connected with the generation of NO through the reactions with OH, HO_2 and O_2 as the reactions (30)–(32).

The removal of SO_2 by radicals may be considered as the reactions (36)–(40) [10,17]. SO_2 can be oxidized to SO_3 by the O radical, which can form sulfuric acid in the presence of water vapor as the reaction (40). OH radical can also convert SO_2 to sulfuric acid via reactions (37) and (38). The reaction of HSO_3 with O_2 produces SO_3 that can be converted into sulfuric acid.

As shown in Table 3, the final products in this process are nitric acid and sulfuric acid, and these acids can be neutralized by a basic material injected at the reactor inlet to form solid salts. This process usually uses ammonia as the basic material to neutralize the nitric and sulfuric acids according to the reactions below:

Table 3
Reactions considered for the model development

Reactions	Rate coefficient[a]	Reaction number
$NO + O \rightarrow NO_2$	$k_1 = 5.0 \times 10^{-33} \exp(900/T)[M]$	(23)
$NO + OH \rightarrow HNO_2$	$k_2 = 7.4 \times 10^{-31}(T/300)^{-2.4}[M]$	(24)
$HNO_2 + OH \rightarrow NO_2 + H_2O$	$k_3 = 1.8 \times 10^{-11} \exp(-390/T)$	(25)
$NO_2 + OH \rightarrow HNO_3$	$k_4 = 2.6 \times 10^{-30}(T/300)^{-2.7}[M]$	(26)
$NO + HO_2 \rightarrow NO_2 + OH$	$k_5 = 3.7 \times 10^{-12} \exp(240/T)$	(27)
$NO + O_3 \rightarrow NO_2 + O_2$	$k_6 = 2.3 \times 10^{-12} \exp(-1450/T)$	(28)
$NO_2 + O \rightarrow NO + O_2$	$k_7 = 1.7 \times 10^{-11} \exp(-300/T)$	(29)
$N + OH \rightarrow NO + H$	$k_8 = 5.8 \times 10^{-11}$	(30)
$N + HO_2 \rightarrow NO + OH$	$k_9 = 2.2 \times 10^{-11}$	(31)
$N + O_2 \rightarrow NO + O$	$k_{10} = 4.4 \times 10^{-12} \exp(-3220/T)$	(32)
$N + NO \rightarrow N_2 + O$	$k_{11} = 3.25 \times 10^{-11}$	(33)
$NO_2 + N \rightarrow N_2O + O$	$k_{12} = 3.0 \times 10^{-12}$	(34)
$2NO_2 + H_2O \rightarrow HNO_2 + HNO_3$	$k_{13} = 1.49 \times 10^{-37}$	(35)
$SO_2 + O \rightarrow SO_3$	$k_{14} = 4.0 \times 10^{-32} \exp(-1000/T)[M]$	(36)
$SO_2 + OH \rightarrow HSO_3$	$k_{15} = 5.0 \times 10^{-31} \exp(300/T)^{3.3}[M]$	(37)
$HSO_3 + OH \rightarrow H_2SO_4$	$k_{16} = 9.8 \times 10^{-12}$	(38)
$HSO_3 + O_2 \rightarrow SO_3 + HO_2$	$k_{17} = 1.34 \times 10^{-12} \exp(-330/T)$	(39)
$SO_3 + H_2O \rightarrow H_2SO_4$	$k_{18} = 6.0 \times 10^{-15}$	(40)

[a] Cited from Atkinson et al. [23]; unit, $cm^3/(molecules\,s)$; M, three-body reaction partner.

$$NH_3 + HNO_3 \rightarrow NH_4NO_3 \quad (41)$$

$$2NH_3 + H_2SO_4 \rightarrow (NH_4)_2SO_4 \quad (42)$$

The reactions (41) and (42) can be assumed to occur instantaneously because acid–base neutralization is usually very fast.

When ammonia is used, SO_2 can readily be removed even without corona discharge. The elementary reactions related to this removal may be expressed as follows [24]:

$$NH_3 + SO_2 \rightarrow NH_3SO_2 \quad (k_{19} = 5.1 \times 10^{-16}) \quad (43)$$

$$NH_3SO_2 + NH_3 \rightarrow (NH_3)_2SO_2 \quad (44)$$

$$(NH_3)_2SO_2 + \tfrac{1}{2}O_2 \rightarrow NH_4SO_3NH_2(s) \quad (45)$$

$$NH_4SO_3NH_2 + H_2O \rightarrow (NH_4)_2SO_4(s) \quad (46)$$

Gas phase chemical reactions mentioned above can form ammonium sulfate as well. According to the literature, the removal of SO_2 due to these reactions is much greater rather than that due to the radical reactions (36)–(40). Since the data available is very limited, it was assumed that the reactions (44)–(46) take place immediately once NH_3SO_2 is formed by the reaction (43). However, this assumption does not affect the prediction for the concentration variations of SO_2.

According to the reactions (41)–(46), the ammonia concentration at any position of the reactor is equated as

$$[NH_3] = [NH_3]_0 - [HNO_3] - 2([H_2SO_4] + [NH_3SO_2]) \quad (47)$$

The radicals produced by corona discharge can disappear through recombination, and generate other active species such as HO_2 and O_3. The radical disappearance reactions considered are tabulated as Table 4. These reactions do not contribute to the removal of NO and SO_2, but take place competitively with one another. Therefore, the removal rate will be depreciated due to such unwanted reactions. When these reactions are not considered in the model, the removal of NO and SO_2 is incorrectly predicted to be finished within a few hundred microseconds [4]. Therefore, to describe this process correctly, the radical disappearance via undesired reactions the likes of recombination should be taken into account in the model.

2.4. Mathematical model

When the space time (reactor volume/gas flow rate) is τ and the pulse frequency is f, the total number of pulses accepted by gas stream becomes $f\tau$, i.e. the gas stream is processed by $f\tau$ pulses [18]. In a corona discharge reactor,

Table 4
Radical disappearance reactions in the corona reactor

Reactions	Rate coefficients at 300 K[a]	Reaction number
$OH + OH \rightarrow H_2O_2$	$k_{20} = 6.5 \times 10^{-31}[M]$	(48)
$OH + O_3 \rightarrow HO_2 + O_2$	$k_{21} = 5.4 \times 10^{-14}$	(49)
$O + OH \rightarrow H + O_2$	$k_{22} = 3.3 \times 10^{-11}$	(50)
$H + O_2 \rightarrow HO_2$	$k_{23} = 5.5 \times 10^{-32}[M]$	(51)
$OH + HO_2 \rightarrow H_2O + O_2$	$k_{24} = 1.1 \times 10^{-10}$	(52)
$O + HO_2 \rightarrow OH + O_2$	$k_{25} = 5.6 \times 10^{-11}$	(53)
$O + O_2 \rightarrow O_3$	$k_{26} = 5.6 \times 10^{-34}[M]$	(54)
$H + O_3 \rightarrow OH + O_2$	$k_{27} = 2.8 \times 10^{-11}$	(55)
$H + HO_2 \rightarrow 2OH$	$k_{28} = 5.7 \times 10^{-11}$	(56)
$OH + OH \rightarrow H_2O + O$	$k_{29} = 1.9 \times 10^{-12}$	(57)
$OH + H_2O_2 \rightarrow H_2O + HO_2$	$k_{30} = 1.1 \times 10^{-12}$	(58)
$O + O_3 \rightarrow 2O_2$	$k_{31} = 8.3 \times 10^{-15}$	(59)

[a] Cited from Atkinson et al. [23]; unit, $cm^3/(molecules\,s)$; M, three-body reaction partner.

ionized gas molecules induce a gas convection in the radial direction, so-called "corona wind" [9]. Due to this corona wind, the reactor can be assumed to be a series of many mixed reactors whose number is $f\tau$. A series of many mixed reactors can be treated as a plug flow reactor, and a material balance of any component can be written in an integrated form as follows:

$$[C_j]_i = [C_j]_{i-1} + \int_0^{\tau_p} R_{j,i}\,\mathrm{d}t \quad (i = 1, 2, 3, \ldots, f\tau - 1, f\tau) \tag{60}$$

where $[C_j]_{i-1}$ and $[C_j]_i$ is the concentration of jth component before and after subjected to ith pulse, and τ_p the pulse period given by

$$\tau_p = \frac{1}{f} \tag{61}$$

In Eq. (60), the reaction rate of jth component at ith pulsing in terms of disappearance can be written as follows:

$$R_{j,i} = \sum \text{disappearance reaction} - \sum \text{generation reaction} \tag{62}$$

For example, referring to Table 3, the net disappearance rate of NO is equated as follows:

$$\begin{aligned} R_{NO} = {} & k_1[NO][O] + k_2[NO][OH] + k_5[NO][HO_2] \\ & + k_6[NO][O_3] - k_7[NO_2][O] - k_8[N][OH] \\ & - k_9[N][HO_2] - k_{10}[N][O_2] + k_{11}[N][NO] \end{aligned} \tag{63}$$

To obtain the concentrations of relevant components at the reactor outlet ($f\tau$), Eq. (60) should be extended from $i = 1$ to $i = f\tau$ for all the components present, and solved simultaneously. Eq. (60) may be solved numerically with the commercial FORTRAN subroutine IVPAG in the International Mathematical and Statistical Library (IMSL). The OH, O, H and N concentrations produced at ith pulsing ($i = 1, 2, 3, \ldots, f\tau - 1, f\tau$) can be equated as Eq. (22) if each pulsing produces an identical amount of radicals. The concentrations of the other components at the inlet of the reactor are:

$$\begin{aligned} & [NO] = [NO]_0, \quad [NO_2] = [NO_2]_0, \quad [N_2O] = 0, \\ & [HNO_2] = 0, \quad [HNO_3] = 0, \quad [SO_2] = [SO_2]_0, \\ & [SO_3] = 0, \quad [HSO_3] = 0, \quad [H_2SO_4] = 0, \\ & [H_2O_2] = 0, \quad [HO_2] = 0, \quad [O_3] = 0 \end{aligned} \tag{64}$$

3. Experimental

3.1. Procedure

The reactor used here has a wire-cylinder electrode structure. The central stainless steel wire (diameter: 0.5 mm) and the outer cylinder (inner diameter: 7 cm) were used as the anode and the cathode, respectively. A positive high voltage pulse was applied to the central wire with the outer cylinder grounded. The effective length of the reactor, i.e. the region that corona discharge covers is 3 m. Fig. 2 shows the schematic diagram of the experimental apparatus. A feed gas stream composed of N_2, O_2, H_2O, NO, SO_2 and NH_3 enters the inlet of the corona reactor, as shown in Fig. 2. The total flow rate of the mixed gas was 10 l/min, varying in the range of 5–10 l/min. The contents of N_2 and O_2 that are major constituents of the gas stream were adjusted by flow meters so that the total flow rate remained unchanged, and the concentrations of NO, SO_2 and NH_3 were controlled by a mass flow controller (model 1179, MKS Instruments Inc.). The content of H_2O was varied by using its vapor pressure, i.e. by changing the temperature of the water bath in which a bottle containing water was immersed. The reactor temperature was kept slightly higher than that of the mixed gas entering the reactor so as to prevent the water vapor from condensing. Table 5 summarizes the detailed experimental conditions of this study.

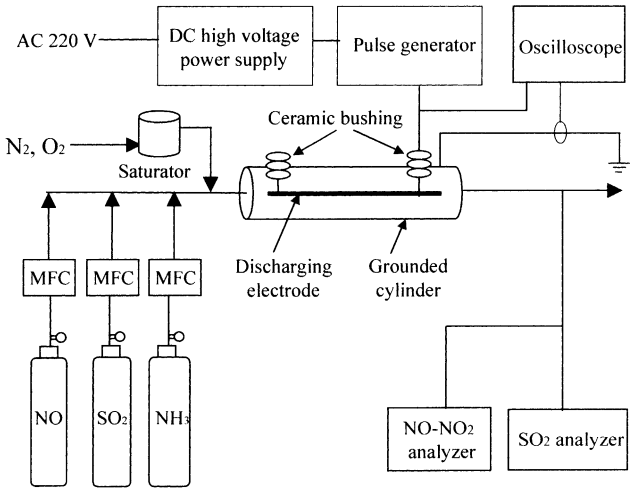

Fig. 2. Schematic representation of the experimental apparatus.

The concentrations of NO and NO_2 were analyzed at the reactor outlet before and after pulsed corona discharge by a chemiluminescence NO–NO_2–NO_x analyzer (model 42H, Thermo Environmental Instrument Inc.). For the analysis

Table 5
Experimental conditions

Variable (unit)	Typical value	Range
Flow rate (l/min)	10	10
$[NO_x]_0$ ($[NO]_0 + [NO_2]_0$) (ppm)[a]	211 (165 + 46)	100–211
$[SO_2]_0$ (ppm)[a]	254	254
$[NH_3]_0$	0–575	0–575
H_2O content (% (v/v))	2	0–5
O_2 content (% (v/v))	20	10–20
Pulse repetition rate (Hz, pulses/s)	0–38	0–50
Charging voltage (kV)	25	15–25

[a] ppm: parts per million, volumetric.

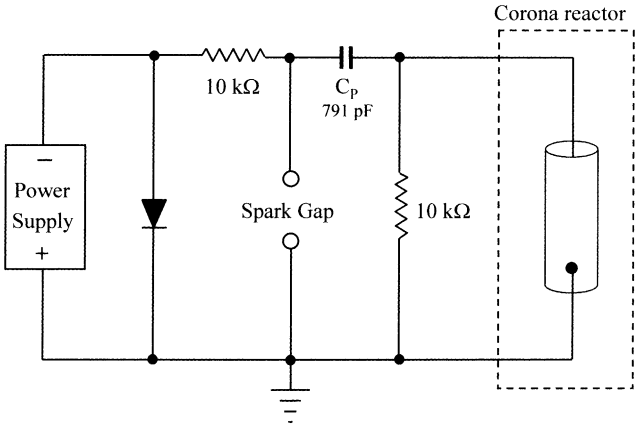

Fig. 3. Circuit of the high voltage pulse generator.

of SO_2 concentration, a pulsed fluorescent SO_2 analyzer (model 43C, Thermo Environmental Instrument Inc.) was employed.

3.2. Pulse forming circuit and measurements

Fig. 3 shows the circuit of the high voltage pulse generator. The negative dc high voltage power supply (Glassmann High Voltage Inc.) charges the capacitor C_p (791 pF) until the voltage on the capacitor reaches the spark-over voltage of the spark gap electrode acting as switch. When the spark gap switch is closed as a result of spark-over, the energy stored in the capacitor is delivered to the corona reactor, producing a narrow high voltage pulse. The charge stored on capacitor C_p flows through a stray inductance to charge the capacitance of the reactor electrode structure. The corona reactor may be electrically described by a capacitor until the corona starts, while during corona development, the reactor should be represented by a non-linear resistor in parallel with a varying capacitor [2]. When the voltage across the electrode structure reaches the corona onset value, corona discharge occurs from the discharging wires. The capacitor was typically charged to a voltage of 25 kV, and it was varied in the range of 15–25 kV. The pulse repetition rate was changed from 10 to 38 Hz (pulses/s).

For voltage measurement, a high voltage probe (Tektronix P6015) having dc attenuation of 1000:1 ± 3% was used with a digital oscilloscope (Tektronix TDS 620B) of which bandwidth and sample rate are 500 MHz and 2.5 GS/s. For current measurement, a current transformer (Tektronix CT-4), a current probe (Tektronix A6302) and a current amplifier (Tektronix AM503B) were used. The A6302 current probe covers frequencies up to 50 MHz. The CT-4 is a high current transformer that extends the measurement capability of the current probe. The current probe was connected to the current amplifier which amplifies the current sensed by the current probe and converts it to a proportional voltage that is displayed on the oscilloscope. Due to the characteristics of the spark gap pulse generator used here, each pulsing produces slightly different waveforms. Therefore, at least 1000 waveforms acquired were averaged for the calculation of the energy.

4. Results and discussion

4.1. Typical waveforms and radical concentrations

Typical voltage and current waveforms are presented in Fig. 4. The pulse voltage can be characterized by its peak value and rise rate. The peak voltage measured at the discharging electrode was 27 kV with a rise rate of 1.3 kV/ns. The current was measured to be 80 A at the maximum and it was extinguished in about 200 ns. The energy delivered to the corona reactor was calculated to be 90.4 mJ/pulse by integrating the product of the voltage and current waveforms.

The radical production efficiency is affected by the electric field because the dissociation rate constants of gaseous molecules k_{d1}–k_{d4} depend on it. We assumed that the electric field is equal to the critical field as a result of balance between ionization and attachment [12]. The calculation of Eqs. (5)–(9) was carried out at this critical reduced electric field of 120 Td (1 Td $= 10^{-21}$ V m^2/molecules). When the reactor volume and the pulse energy delivered to the reactor are known, the concentrations of OH, O, H and N radicals produced per pulse can be calculated by Eq. (22).

4.2. Comparison of experimental results with the model

Unless otherwise mentioned, the inlet concentrations of NO and NO_2 and the contents of O_2 and H_2O are as shown as typical values in Table 5.

4.2.1. Effect of initial concentration

Fig. 5 shows the effect of initial NO_x ($NO+NO_2$) concentration on the conversion of NO where the calculation results

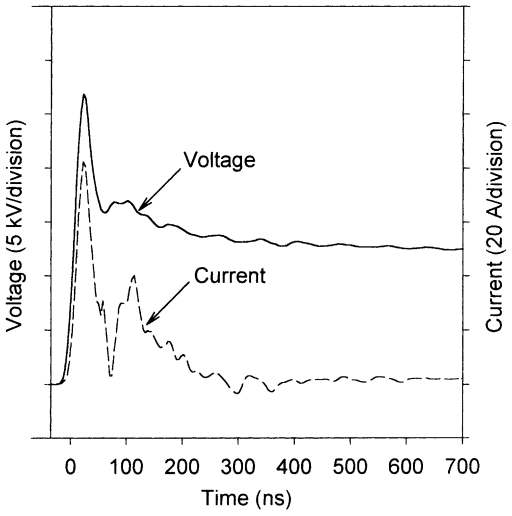

Fig. 4. Typical voltage and current waveforms.

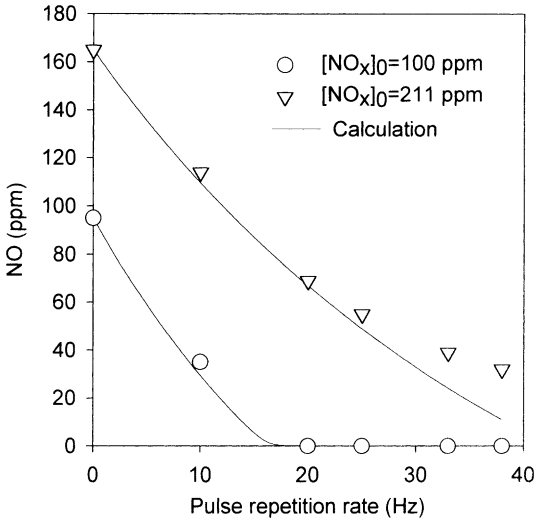

Fig. 5. Effect of the initial concentration on the conversion of NO.

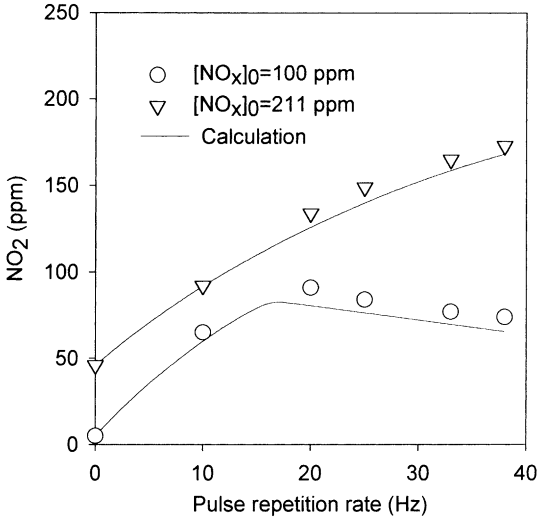

Fig. 6. Effect of the initial concentration on the concentration of NO_2 at the outlet.

are also shown. A couple of experiments for the change in the initial NO_x ($NO + NO_2$) concentration were performed at 100 and 211 ppm. This change in the initial concentration did not affect the energy delivered to the reactor because a few hundred ppm was too low to affect the discharge characteristics. The pulse repetition rate can be changed by varying the charging time of the capacitor C_p in the pulse generation circuit (Fig. 3). The output voltage and current from the dc high voltage power supply were varied in order to change the charging time. One trend of Fig. 5 is that the concentration of NO decreased with the pulse repetition rate because the radicals capable of converting NO were produced more frequently as the pulse repetition rate increased. When the initial concentration was 100 ppm, NO decreased almost linearly with the pulse repetition rate, and it was completely depleted at a pulse repetition rate around 20 Hz. As explained above, the concentrations of radicals produced per pulse are constant, and thus, the increase in the initial concentration of NO_x resulted in higher NO concentration at the reactor outlet because the radicals available for the conversion of NO were relatively small. However, the reaction rate increases with the concentration of reactants because it is expressed as functions of both rate coefficient and concentration, and as expected, the amount of NO converted into NO_2 increased with the initial concentration (Fig. 6). The proposed model adequately predicted the experimental data.

4.2.2. Effect of humidity

The dependency of the conversion of NO on the H_2O content is depicted in Fig. 7. Increase in the H_2O content decreased the conversion rate, which can be explained as follows. Firstly, OH radical produced from H_2O can deplete ozone as follows [23]:

$$OH + O_3 \rightarrow HO_2 + O_2 \quad (65)$$

According to our previous study, ozone produced during corona discharge plays a key role in the oxidation of NO [25,26]. The increase in the H_2O content gives rise to the increase in the production of OH radical. This increase in the concentration of OH radical hampers the formation of ozone, which results in the decrease in the oxidation of NO. As shown in Fig. 8, nitric oxide can be converted to NO_2 in the absence of water vapor, which may serve as an evidence that ozone plays an important role in the oxidation chemistry. We remind the reader that NO can react with O radical and ozone. In other words, NO can be converted in the absence of water vapor if oxygen is present in the gas stream. Secondly, the energy delivered to the corona reactor per pulse decreases with the increase in the H_2O content. The energy delivered per pulse was 102, 90.4 and 84 mJ at 0, 2 and 5% (v/v) of the H_2O content, respectively. Dissociative attachment ($e + H_2O \rightarrow OH + H^-$) can explain the decrease in the pulse

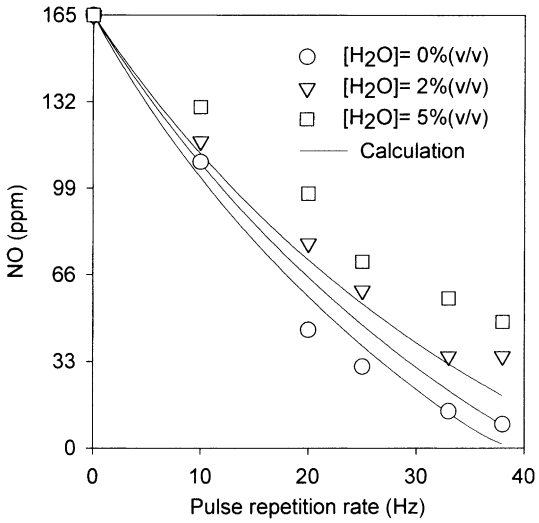

Fig. 7. Effect of the humidity on the conversion of NO ($[NO]_0 = 165$ ppm and $[NO_2]_0 = 46$ ppm).

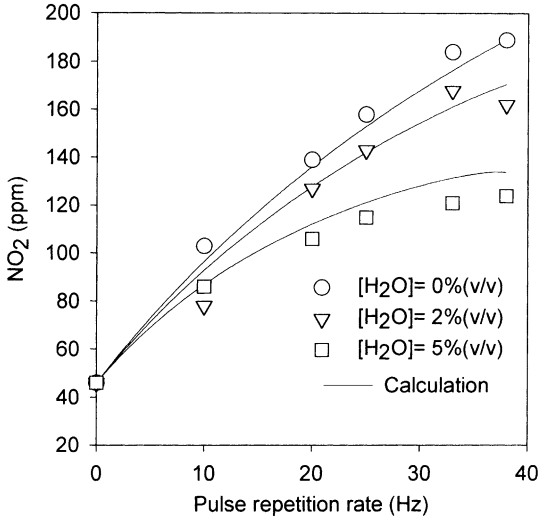

Fig. 8. Effect of the humidity on the concentration of NO_2 at the outlet ($[NO]_0 = 165$ ppm and $[NO_2]_0 = 46$ ppm).

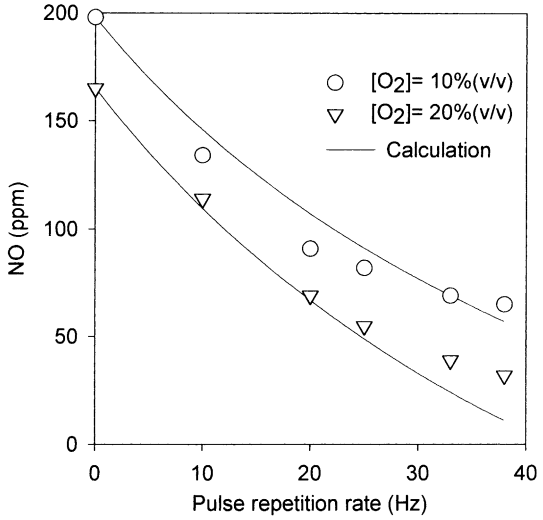

Fig. 9. Effect of the oxygen content on the conversion of NO ($[NO]_0 = 198$ ppm and $[NO_2]_0 = 13$ ppm at 10% (v/v) O_2; $[NO]_0 = 165$ ppm and $[NO_2]_0 = 46$ ppm at 20% (v/v) O_2).

current, i.e. the energy delivered [10,14]. The concentrations of the radicals produced are proportional to the energy delivered, and as a result the decrease in the energy delivered decreases the rate of the conversion of NO. The model was able to track the trend of the NO conversion according to the variations in the humidity, but the effect of the humidity was more significant than the model predicted. In the mean time, the concentration of NO_2 was lower when the H_2O content was higher, as depicted in Fig. 8. The OH radical causes the further oxidation of NO_2 to nitric acid as the reaction (26), which may explain why the increase in H_2O content gives rise to the decrease in the concentration of NO_2.

4.2.3. Effect of oxygen concentration

The oxygen concentration may hold an important position in the gas composition for the conversion of NO because it is deeply involved in the production of reactive components such as O, OH and O_3. In addition, the variation of oxygen content influences the pulse properties such as peak current, pulse width and voltage rising time because oxygen has large electron attachment coefficient [14]. Since the electron attachment process reduces the number of electrons, the pulse current decreases with the oxygen content. The decrease in the current surely decreases the energy delivered to the reactor. The experiments were carried out by changing the oxygen content from 10 to 20% (v/v) with the other variables kept constant as in Table 5. Figs. 9 and 10 show the effect of oxygen content on the concentrations of NO and NO_2 at the reactor outlet. The energy delivered per pulse reduced from 114.8 to 90.5 mJ when the oxygen content was increased from 10 to 20% (v/v), respectively. Nevertheless, the increase in the oxygen content increased the conversion of NO, as shown in Fig. 9. This result indicates that the oxidation radicals mentioned above mainly cause the conversion of NO. Considerable amount of N radical can also be produced in this system, and NO can be reduced to N_2 according to the reaction (33). However, NO can be generated by the reactions (30)–(32). Due to such counteraction, most of NO converted was oxidized to NO_2, as shown in Fig. 10. In other words, the reduction of NO to N_2 by N radical almost offset the generation of NO, and thus, the net effect of N radical on the reduction of NO is minor.

4.2.4. Effect of peak voltage

Fig. 11 represents the conversion of NO according to the variations of the charging voltage of the capacitor C_p at a fixed flow rate of 5 l/min. We emphasize that the increase in charging voltage increases the energy delivered per pulse

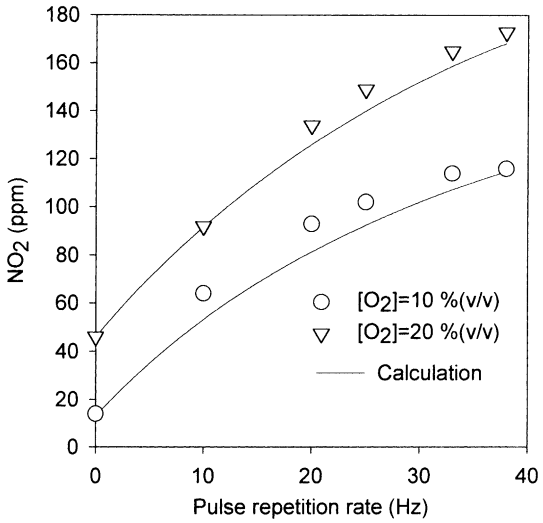

Fig. 10. Effect of the oxygen content on the concentration of NO_2 at the outlet ($[NO]_0 = 198$ ppm and $[NO_2]_0 = 13$ ppm at 10% (v/v) O_2; $[NO]_0 = 165$ ppm and $[NO_2]_0 = 46$ ppm at 20% (v/v) O_2).

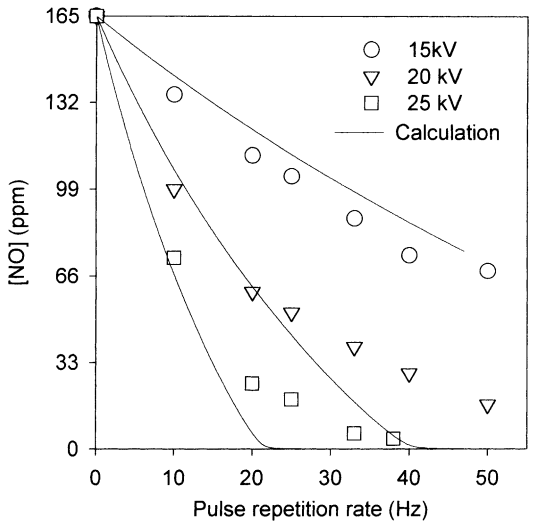

Fig. 11. Dependency of the conversion of NO on the peak voltage ($[NO]_0 = 165$ ppm).

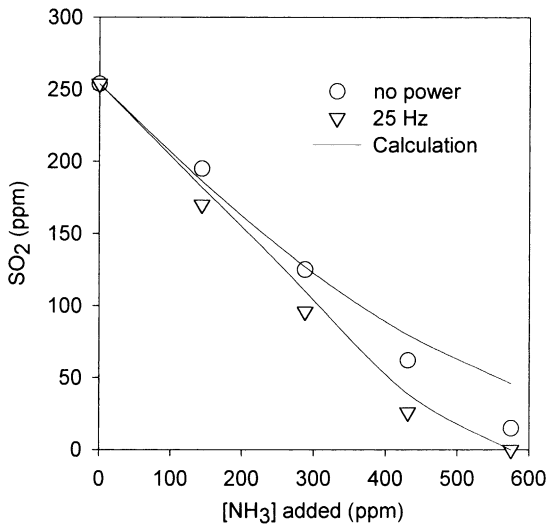

Fig. 13. Effect of the ammonia concentration on the removal of SO_2 ($[SO_2]_0 = 254$ ppm).

as well as the peak voltage. When the charging voltage was 15, 20 and 25 kV, the energy delivered per pulse was 17, 48 and 90.4 mJ. As can be seen in Eq. (22), the concentrations of radicals produced per pulse increase with the energy delivered per pulse, and we can observe that the concentration at the reactor outlet was lower at higher voltage. The model calculations showed good agreements with the experimental data. These good agreements indicate that the important thing in this process is not the charging voltage itself, but the increase in the energy delivery due to the increase in the charging voltage.

4.2.5. Effect of flow rate

Fig. 12 shows the concentration of NO measured at the reactor outlet when the flow rate was varied from 5 to 10 l/min.

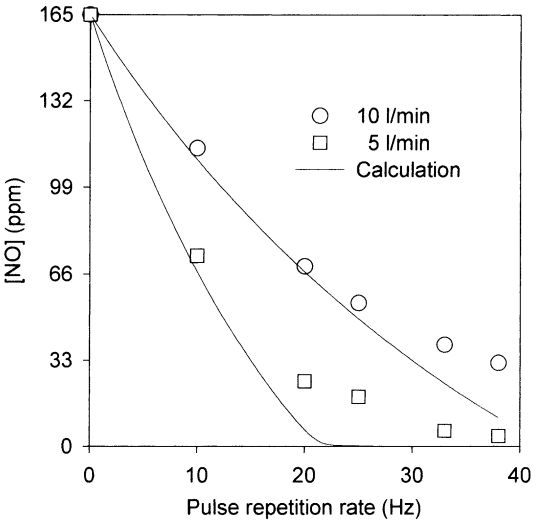

Fig. 12. Dependency of the conversion of NO on the gas flow rate ($[NO]_0 = 165$ ppm).

An increase in the gas flow rate gives rise to a decrease in the space time, i.e. the total number of pulses accepted by the gas stream decreases with the increase in the flow rate. Therefore, the concentration of NO at the reactor outlet increased as the flow rate increased. The model calculation results overestimated the removal, especially at higher frequency. Such discrepancy can be seen in Figs. 5, 7, 9 and 11 as well. In this model, axial dispersion in the corona reactor was not considered, which may account for this overestimation. In a corona discharge system, ionized gas molecules can induce a gas convection, the so-called "corona wind" [9]. The influence of this phenomenon on the gas flow has widely been studied for electrostatic precipitator (ESP) [27–29]. Since the pulsed corona discharge process is operated at higher electric field than ESP and the power is supplied in a pulse mode, the gas flow would more significantly be affected by the corona wind. In the future, the effect of the gas flow on the concentration profile should be taken into account in the model.

4.2.6. Effect of ammonia concentration

Pulsed corona discharge process generally uses ammonia to form ammonium salts as the final products of SO_2 and NO removal. The effect of ammonia on the concentration of SO_2 at the reactor outlet was examined and the results are presented in Fig. 13. In this experiment, the concentration of ammonia was varied up to 575 ppm. As shown in Fig. 13, the concentration of SO_2 was observed to decrease with the increase in the concentration of ammonia. Even in the absence of corona discharge, considerable amount of SO_2 was removed by the gas phase reactions (43)–(46). Although the removal of SO_2 was promoted at a pulse repetition rate of 25 Hz, it was not significant. In other words, the removal of SO_2 is mainly caused by the reactions with ammonia rather than corona discharge induced by pulsed power. The effect

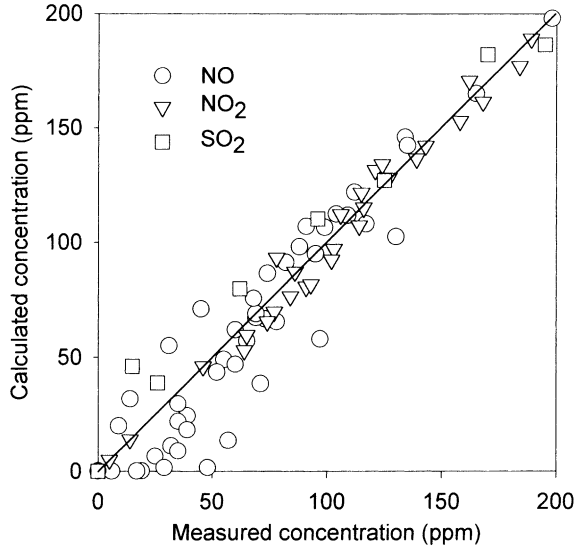

Fig. 14. Comparison between the predicted and measured concentrations.

of ammonia on the conversion of NO was not presented in Fig. 13 since it was negligible. The model was able to estimate well the effect of ammonia concentration both in the presence and in the absence of pulsed corona discharge.

4.2.7. Model verification and validation

Comparisons between the predicted and measured concentrations of NO, NO_2 and SO_2 in Figs. 5–13 were made to verify the validity of the model proposed. Fig. 14 depicts a plot of the measured concentrations versus the calculated concentrations. This figure indicates that the closer the data approach the diagonal, the better the model agrees with the experimental results. As can be seen, the three kinds of symbols (NO, NO_2 and SO_2) are concentrated on the diagonal at high concentration (low removal efficiency) while they are dispersed around it at low concentration (high removal efficiency). These deviations at high concentration may have been arisen from the axial dispersion that was not considered in this model. Nevertheless, the mathematical model proposed was able to adequately predict all of the experimental data over the entire range of the parameters including the peak voltage, the gas flow rate, the oxygen content, the humidity, the ammonia concentration and the initial concentration.

5. Conclusions

In this paper, a mathematical model was proposed to describe the behavior of the pulsed corona discharge process for the removal of nitric oxide and sulfur dioxide. From the proposed model, the concentration variations of NO, NO_2 and SO_2 at the reactor outlet can readily be predicted without using any correlation or adjustable parameters. The model has been tested experimentally, which adequately described the experimental data for the changes in key variables such as initial concentration, humidity, oxygen content, ammonia concentration, peak voltage and the gas flow rate.

References

[1] A. Mizuno, J.S. Clements, R.H. Davis, IEEE Trans. Ind. Appl. 22 (1986) 516.
[2] G. Dinelli, L. Civitano, M. Rea, IEEE Trans. Ind. Appl. 26 (1990) 535.
[3] S. Masuda, H. Nakao, IEEE Trans. Ind. Appl. 26 (1990) 374.
[4] R.P. Dahiya, S.K. Mishra, A. Veefkind, IEEE Trans. Plasma Sci. 21 (1993) 346.
[5] A. Mizuno, K. Shimizu, A. Chakrabarti, L. Dascalescu, S. Furuta, IEEE Trans. Ind. Appl. 31 (1995) 957.
[6] Y. Song, Y. Choi, H. Kim, W. Shin, S. Keel, S. Chung, K. Choi, H. Choi, S. Kim, K. Chang, J. Korea Air Poll. Res. Assoc. 12 (1996) 487.
[7] M. Rea, K. Yan, IEEE Trans. Ind. Appl. 31 (1993) 507.
[8] J.S. Chang, P.A. Lawless, T. Yamamoto, IEEE Trans. Plasma Sci. 19 (1991) 1152.
[9] H. Tamon, H. Mizota, N. Sano, S. Schulze, M. Okazaki, AIChE J. 41 (1995) 1701.
[10] J.J. Lowke, R. Morrow, IEEE Trans. Plasma Sci. 23 (1995) 661.
[11] B.M. Penetrante, M.C. Hsiao, B.T. Merritt, G.E. Vogtlin, P.H. Wallman, IEEE Trans. Plasma Sci. 23 (1995) 679.
[12] W. Sun, B. Pashaie, S.K. Dhali, J. Appl. Phys. 79 (1996) 3438.
[13] L. Civitano, G. Dinelli, F. Busi, M. D'Angelantonio, I. Gallimberti, M. Rea, Electron Beam Processing of Combustion Gases, IAEA-TECDOC-428, 1987, pp. 55–84.
[14] I. Gallimberti, Pure Appl. Chem. 60 (1988) 663.
[15] Y.L.M. Creyghton, Pulsed positive corona discharges, Ph.D. Thesis, Eindhoven University of Technology, Eindhoven, 1994, pp. 72–101.
[16] D. Bhasavanish, S. Ashby, C. Deeney, L. Schlitt, in: Proceedings of the 9th IEEE Pulsed Power Conference, Albuquerque, New Mexico, 1993, pp. 441–444.
[17] L. Civitano, Non-Thermal Plasma Techniques for Pollution Control: Part B, Springer-Verlag, Weinheim, 1993, pp. 103–130.
[18] Y.S. Mok, S.W. Ham, Chem. Eng. Sci. 53 (1998) 1667.
[19] J. Li, W. Sun, B. Pashaie, S.K. Dhali, IEEE Trans. Plasma Sci. 23 (1995) 672.
[20] M.B. Chang, J.H. Balbach, M.J. Rood, M.J. Kushner, J. Appl. Phys. 69 (1991) 4409.
[21] A. Kulikovsky, IEEE Trans. Plasma Sci. 25 (1997) 439.
[22] D.L. Baulch, R.A. Cox, R.F. Hampson Jr., J.A. Kerr, J. Troe, R.T. Watson, J. Phys. Chem. Ref. Data 9 (1980) 295.
[23] R. Atkinson, D.L. Baulch, R.A. Cox, R.F. Hampson Jr., J.A. Kerr, J. Troe, J. Phys. Chem. Ref. Data 21 (1992) 1125.
[24] E.M. Hartley Jr., M.J. Matteson, Ind. Eng. Chem. Fundam. 14 (1975) 67.
[25] Y.S. Mok, I. Nam, Chem. Eng. Technol. 22 (1999) 527.
[26] Y.S. Mok, I. Nam, R.W. Chang, S.W. Ham, C.H. Kim, Y.M. Jo, in: Proceedings of the 7th International Conference on Electrostatic Precipitation, Hilton, Kyungju, Korea, 1998, pp. 270–277.
[27] S. Oglesby, Jr., G.B. Nichols, Electrostatic Precipitation, Marcel Dekker, New York, 1978.
[28] T. Yamamoto, H.R. Velkoff, J. Fluid Mech. 108 (1981) 1.
[29] Y.S. Cho, S.J. Yoa, J. Korea Air Poll. Res. Assoc. 12 (1996) 243.